


Molecular characterization of aviadenovirus serotypes and pathogenicity of the identified adenovirus in broiler chickens

Mohamed Lebdah,^{*} Dalal S. Alshaya,[†] Areej S. Jalal,[†] Mohamed R. Mousa,[‡] Mohamed M. Radwan,[§] Mahmoud Samir,[#] Amany Adel,[#] Najah M. Albaqami,^{||} Mohamed T. El-Saadony,[¶] Khaled A. El-Tarabily ,^{**,††,‡‡,1} and Yara F. H. El basrey^{*}

^{*}Department of Avian and Rabbit Medicine, Faculty of Veterinary Medicine, Zagazig University, Zagazig, 44511, Egypt; [†]Biology Department, College of Science, Princess Nourah bint Abdulrahman University, Riyadh, 11671, Saudi Arabia; [‡]Department of Pathology, Faculty of Veterinary Medicine, Cairo University, Giza, 11361, Egypt; [§]Department of Virology, Faculty of Veterinary Medicine, Cairo University, Giza, 11361, Egypt; [#]Reference Laboratory for Veterinary Quality Control on Poultry Production, Animal Health Research Institute, Agriculture Research Center, Giza, 12618, Egypt; ^{||}Department of Biological Sciences, Zoology, King Abdulaziz University, Jeddah, 21589, Saudi Arabia; [¶]Department of Agricultural Microbiology, Faculty of Agriculture, Zagazig University, Zagazig, 44511, Egypt; ^{**}Department of Biology, College of Science, United Arab Emirates University, Al-Ain, 15551, United Arab Emirates; ^{††}Khalifa Center for Genetic Engineering and Biotechnology, United Arab Emirates University, Al-Ain, 15551, United Arab Emirates; and ^{‡‡}Harry Butler Institute, Murdoch University, Murdoch, Western Australia, 6150, Australia

ABSTRACT Inclusion body hepatitis (IBH) is an economically significant viral disease that primarily affects broiler chickens. At least 12 different aviadenovirus serotypes are responsible for causing IBH. This study aimed to use polymerase chain reaction (PCR) and phylogenetic analysis to characterize fowl adenovirus isolates that were in circulation from 2019 to 2021 and investigate the pathogenicity of the isolated strains in commercial broiler chickens. Suspected liver samples were molecularly identified using hexon gene targeting by PCR, and viruses were isolated using chick embryo liver cell culture. For serotype identification, the fowl adenovirus-positive samples were

subjected to hexon gene sequencing and phylogenetic analysis. The pathogenicity of two isolates was tested in commercial chickens via the oral route. The phylogenetic analysis of the hexon gene showed that the isolated viruses clustered with serotype 8a species E. On testing the pathogenicity of the isolates based on necropsy and histopathological examination, no mortality was observed; however, lesions were observed in the liver, kidney, heart, pancreas, bursa, and lung specimens with intermittent virus shedding at different time points throughout the experimental period. Further research on the likelihood of vaccine production is warranted to limit disease-related losses.

Key words: fowl adenovirus, hexon gene, inclusion body hepatitis, pathogenicity, phylogenetic analysis

2022 Poultry Science 101:101918

<https://doi.org/10.1016/j.psj.2022.101918>

INTRODUCTION

The poultry sector continues to grow and industrialize in many parts of the world. This increases the chances of disease transmission and causes substantial economic losses, particularly in the absence of vaccine control. Adenovirus infections are caused by non-enveloped icosahedral viruses of the genus

aviadenovirus in the family adenoviridae with linear double-stranded DNA ranging in size from 25 to 46 kbp (Benko et al., 2005; Adair and Smyth, 2008).

Adenoviruses isolated from poultry were classified into five fowl adenovirus (FAdv) species, FAdV-A-E represented by 12 types FAdV-1–8a and FAdV-8b–11 (Harrach and Kajan, 2011; Fitzgerald et al., 2020). Adenovirus strains are found all over the world, and different types/species have been discovered in different geographic localities (Schachner et al., 2014; Niczyporuk, 2016). Inclusion Body Hepatitis (IBH) can be caused by any adenovirus type or species, but the adenoviruses FAdV-2/D, FAdV-8a/E, FAdV-8b/E, and FAdV-11/D are the most commonly implicated types in

© 2022 The Authors. Published by Elsevier Inc. on behalf of Poultry Science Association Inc. This is an open access article under the CC BY-NC-ND license (<http://creativecommons.org/licenses/by-nc-nd/4.0/>).

Received December 9, 2021.

Accepted April 4, 2022.

¹Corresponding author: ktarabily@uaeu.ac.ae

this disease, which is characterized by intranuclear inclusion bodies in hepatocytes and liver hemorrhages (Zhao et al., 2016; Schachner et al., 2018).

FAdV-1/A is the primary cause of gizzard erosion (Hess, 2013; Fitzgerald et al., 2020). Furthermore, epidemiological studies confirmed that FAdV-4/C is responsible for hydropericardium hepatitis syndrome (Niu et al., 2018; Schachner et al., 2018), which can have a significant impact on poultry health and contribute to economic losses in the poultry industry globally. Egypt currently has a large number of positive cases of adenovirus infections in poultry flocks and commercial IBH vaccines are not currently available in Egypt. Autogenously FAdV broiler vaccines specific for the exact strain in infected flocks have been used in many areas where IBH outbreaks have occurred.

The characterization of adenovirus strains at the molecular level is an ongoing process. However, FAdV serotypes D (2 and 11) and FAdV serotype E (8a) have been well characterized (Elbestawy et al., 2020; El basrey et al., 2020). Immunosuppression caused by infectious bursal disease virus or chicken anemia virus (Choi et al., 2012; Eregae et al., 2014) and Marek's disease (Niczyporuk, 2016) is believed to be a cofactor in IBH cases in chickens (Meng et al., 2018; Su et al., 2018). However, recent research, suggests that immunosuppressive factors may not be required for disease induction in chickens based on adenovirus isolates (Morshed et al., 2017).

The primary objective of the current study was to detect and characterize adenovirus strains associated with IBH in affected flocks, and investigate pathogenicity in commercial broiler chickens.

MATERIALS AND METHODS

Specimens' Collection and Processing

Between January 2019 and January 2020, liver samples were collected from 15 broiler flocks (three birds per flock) in various locations throughout Sharkia Governorate, Egypt. The flocks were 19 to 40 days old and had a mortality rate of 5 to 10%. A postmortem examination was performed, and liver samples were obtained. Liver samples from each flock were combined and minced in phosphate-buffered saline (PBS) with a W/V ratio of 1:10. The homogenates were centrifuged at $8,000 \times g$ for 10 min., and the supernatant was collected for DNA extraction.

The Institutional Animal Care and Use Committee of Zagazig University, Zagazig, Egypt approved this study. All institutional and national guidelines for the care and use of birds were adhered to while conducting this study.

Molecular Identification by Polymerase Chain Reaction (PCR)

DNA was extracted following the *EasyPure* Viral DNA/RNA Kit catalogue number ER201-01 (TransGen

Biotech Co., Ltd, Beijing, China). The extracted nucleic acid was stored at -20°C until further use.

The extracted nucleic acid was detected using a primer pair specific for the L1 region of hexon gene of FAdV, by employing the following primer sequence: forward 5' -AAT GTC CAN ACC GAR AAG GC-3' and reverse 5' -CBG CBT RCA TGT ACT GGT A-3' (Zhang et al., 2017). The Thermo PCR master mix catalogue number K0171 (Thermo Fisher Scientific Inc., Waltham, MA, USA) was used for DNA amplification as follows: 12.5 μL of $2\times$ master mix, 1 μL each of forward and reverse primers, 5 μL of DNA, and the reaction was completed by adding up to 25 μL of PCR-grade H_2O .

The thermal profile for the amplification was as follows: 95°C for 5 min, followed by 40 cycles of 95°C for 45 s, 56°C for 45 s, 72°C for 1 min, and 10 min of final extension at 72°C . A gel documentation system was used to electrophorese the PCR products, and the suspected molecular weight was 830 bp.

Virus Isolation

For virus isolation, positive PCR liver samples were frozen and thawed three times before being macerated in 10% W/V PBS and an antibiotic mixture and centrifuged at $8,000 \times g$ for 10 min. The collected supernatant was filtered using a membrane filter (0.22 μm) (Millipore Corporation, Burlington, MA, USA).

According to the manufacturer's instructions, the filtered supernatant was used to inoculate chick embryo liver cell culture (CELC) prepared using 14-day-old specific pathogen free (SPF) chicken embryos (Soumyalekshmi et al., 2014). Inoculation was performed in the CELC culture when liver samples showed 90% confluency. Daily monitoring was conducted for 3 days for the presence of the cytopathic effect (CPE).

Nucleotide Sequencing and Analysis

QIAquick gel extraction kit catalogue number 28704 (Qiagen Digital Insights, Hilden, Germany) was used for the purification of PCR products, which were then sequenced using a BigDye Terminator kit (version 3.1; Applied Biosystems, Foster City, CA, USA). The sequence reactions were purified using DyeEx 2.0 spin purification kit catalogue number 63204 (Qiagen Digital Insights) and then run on an Applied Biosystems 3130 Genetic Analyzer (Foster City, CA, USA) according to the manufacturer's manual.

The nucleotide sequences were designated and submitted to Genbank after being sequenced. Bioedit software was used to align and analyze the nucleotide sequences in the L1 region of the hexon gene. Molecular Evolutionary Genetics Analysis-X software was used to perform the phylogenetic analysis, which used the neighbor-joining method with 1,000 bootstrap replicates.

Titration of FAdV on CELC

In brief, CELC was prepared using 14- to 16-day-old SPF chicken embryos (Soumyalekshmi et al., 2014). Cells were seeded at a density of 1×10^5 and cultured in Dulbecco's Modified Eagle's Medium supplemented with 10% fetal bovine serum and 1% penicillin-streptomycin solution.

Following that, CELCs were inoculated with ten-fold serial dilutions of the virus ranging from 10^{-4} to 10^{-9} with 100 μL of each dilution inoculated into three wells. The final row was designated as the negative control. In 24-well plates of CELC at 90%, the median tissue culture infective dose (TCID₅₀) for each positive sample was determined. For 3 days, the plates were incubated at 37.5°C with 5% CO₂. The CPE was observed on the second day, and the TCID₅₀ was calculated on the third day using the Reed and Muench method (Reed and Muench, 1938).

Experimental Design for Pathogenicity Studies of FAdV Isolates in Commercial Chickens

Commercial broiler chicks that were 121 days old were divided into three equal groups. Throughout the experiment, the groups were housed separately in isolator units with unlimited access to feed and water. On the first day of life, birds from groups A and B were orally inoculated with isolate 1 and 2, respectively, at 10^7 TCID₅₀/mL (Matos et al., 2016a). In contrast, group C birds, remained unvaccinated. Every bird was examined daily to record any clinical signs and mortalities. Three birds from each group were sacrificed at 4, 5, 7, 9, 11, 15, 18, 21, and 24 d after infection.

Throughout the experiment, all sacrificed and dead birds were necropsied and gross lesions in the liver, kidney, heart, pancreas, bursa, and lungs were documented. Cloacal swabs were collected at 3, 5, 7, 11, 15, 21, and 24 d post-inoculation for determining the viral load and shedding using Syber Green-based real-time quantitative PCR.

Histopathology

Liver, kidney, heart, pancreas, bursa, and lung specimens were collected and preserved in 10% neutral buffered formalin before being processed using the routine paraffin embedding technique. The samples were fixed in 10% buffered formalin. For histopathological examination, organs were embedded in paraffin wax for sectioning (5 μm) and routinely stained with eosin and hematoxylin.

For histopathological evaluation, Olympus BH-2 light microscope (Olympus Optical Co. Ltd, Tokyo, Japan) was used after which photographs were taken using a digital camera (Jenoptik ProgRes Camera, C12plus, Frankfurt, Germany).

Detection of Virus Shedding and Viral Load by Syber Green PCR

TransStart Green qPCR Super Mix catalogue number AQ101-01 (TransGen Biotech Co., Ltd) was used to amplify the DNA as follows: 10 μL of 2 \times trans start Green qPCR SuperMix, 0.5 μL of forward and reverse primers, 0.4 μL of passive dye (10 \times), 5 μL of DNA and 20 μL of PCR grade H₂O.

The thermal profile for the amplification was as follows: 94°C for 5 min, the cycling step was repeated for 40 cycles at 94°C for 10 s, 56°C for 1 min, 72°C for 10 s, followed by the dissociation stage. Stratagene Mx3000p was used for reading the PCR amplification results in the form of amplified curves supported by dissociation temperature curve. The primers were identical to those used in conventional PCR.

Statistical Analysis

Statistical Package for Social Sciences version 21.0 for Windows was used for statistical analysis (SPSS Inc., Chicago, IL, USA). The histopathology scores were compared between groups using Fisher's exact test, with a Bonferroni correction for multiple comparisons. Differences were considered significant with $P < 0.05$.

RESULTS

External Examination and Postmortem Lesions of the Investigated Flocks

In different regions of Sharrkia Governorate, Egypt, mortalities in the examined birds ranged from 5 to 10%, which that lasted for 4 days, and gradually declined with ages ranging from 19 to 40 days old due to lethargy and sometimes diarrhea. The liver was the most affected organ on necropsy, with paleness and petechial hemorrhage (Figure 1).

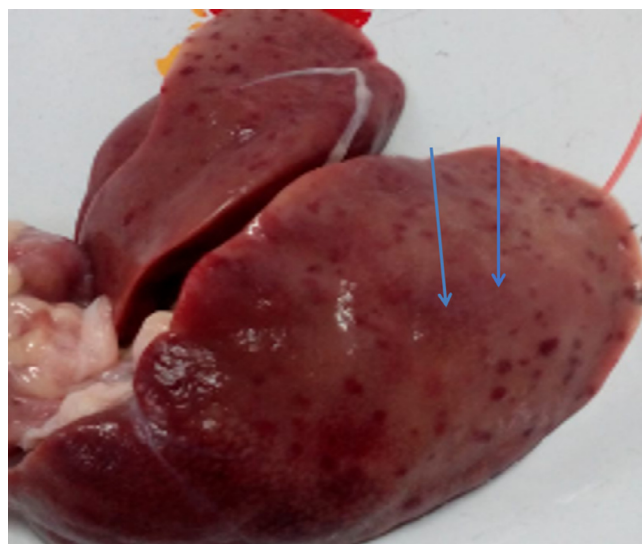


Figure 1. Affected liver of examined birds with petechial hemorrhage.

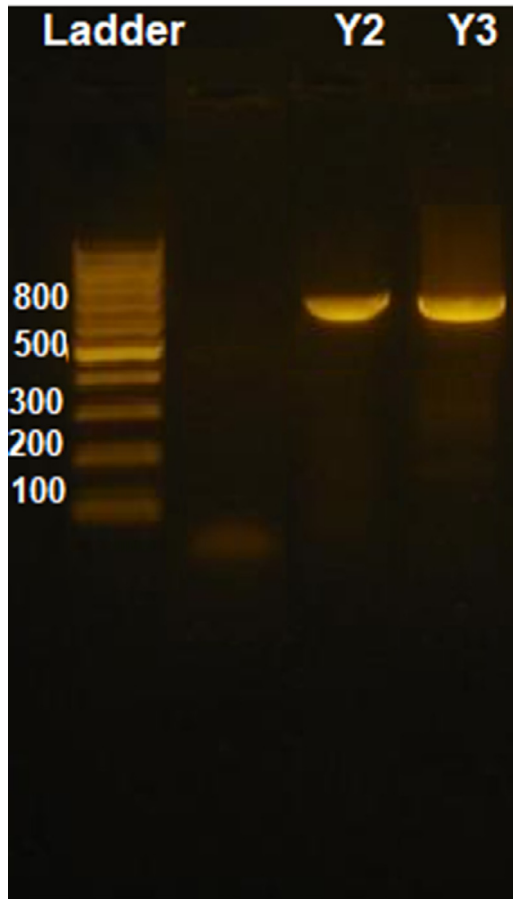


Figure 2. Gel electrophoresis of 830 bp product amplified by polymerase chain reaction using primer set 1 targeting hexon gene. Samples Y2 and 3 are positive.

Molecular Identification of FAdVs by PCR

Only two of the 15 liver samples tested, were PCR positive after screening primer sets targeting the hexon gene, producing an 830 bp band (Figure 2). The hexon gene sequences of the detected FAdVs were submitted to the Genbank database under the accession numbers MW574967 and MW574968.

Virus Isolation

The two isolates displayed varying degrees of CPE on the CELC as early as 48 hours post-infection in the form of rounding, clumping, and cell aggregation.

Gene Sequencing and Phylogenetic Analysis of the Isolated Viruses

Following assembly, the hexon gene sequences of the two FAdVs isolates MW574967 and MW574968 were analyzed so that they could be classified. The FAdVs were classified in the main clade corresponding to the reference species E serotype 8a based on the phylogenetic analysis (Figure 3). The FAdV-E serotype 8a, the examined strains and the reference FAdVs had the highest nucleotide similarity (97.8–98%; Table 1).

Pathogenicity Assessment

Clinical Signs and Gross Lesions Throughout the experiment, chickens inoculated orally with the two identified isolates did not show any clinical signs or mortality. After conducting necropsy of the killed birds at each collection time, the examined liver exhibited paleness with petechial hemorrhage in both inoculated groups at different sample collection times throughout the experiment (Figure 4). In both groups, the kidneys showed paleness, with the presence of hemorrhages.

At 5 and 10 days post-infection (DPI), both groups' hearts showed petechial hemorrhage (Figure 5). Both groups had no gross lesions in the pancreas or the bursa of Fabricius. The lungs were congested and edematous, and the skeletal muscles had petechial hemorrhages on the breast and thigh muscles.

Histopathology

- **Liver:** Normal hepatic plates were found in group C, which also had normal hepatocytes and intact bile canaliculi. Normal hepatic sinusoids were found between the hepatic plates. Hepatic tissue from group A was examined and found to have basophilic intranuclear inclusion bodies in the affected hepatocytes from 4 to 7 DPI as well as mild hepatocytes degeneration and fewer inflammatory cells infiltration. In different sacrifices, group B revealed a large number of intranuclear inclusion bodies (4–15 DPI). In comparison with group A, necrobiotic hepatocytes were more prominent in the hepatic plates of group B, which was associated with an increase in mononuclear inflammatory infiltration that replaced the necrosed hepatocytes (Figure 6).
- **Kidneys:** The normal histological structure of cortical regions containing closely packed nephron, blood vessels, and initial collecting tubules supported by interstitial connective tissue was observed in the kidneys. The medullary cones showed the presence of intact collecting tubules, healthy looped tubules, and ureter branches with supporting blood capillaries and interstitial tissue. Moreover, groups A and B showed histopathological changes in the examined tissue sections from different sacrifices. Interstitial nephritis was observed in groups A and B in different sacrifices that began at 4 DPI. Multifocal to diffuse areas of interstitial nephritis were noted in the renal parenchyma of the cortical and medullary regions with aggregations of mononuclear inflammatory cells that replaced the necrosed renal tubules and the presence of basophilic intranuclear inclusion bodies in the epithelial lining of renal tubules.

Necrosed epithelial lining of the renal tubules appeared more severe and widespread in group B compared to group A which was characterized by pyknotic nuclei with epithelial cell sloughing into the lumen of the affected tubules. Mesangial proliferative glomerulonephritis was observed in group B at 21 to 24 DPI as evidenced by increased affinity to basophilic staining

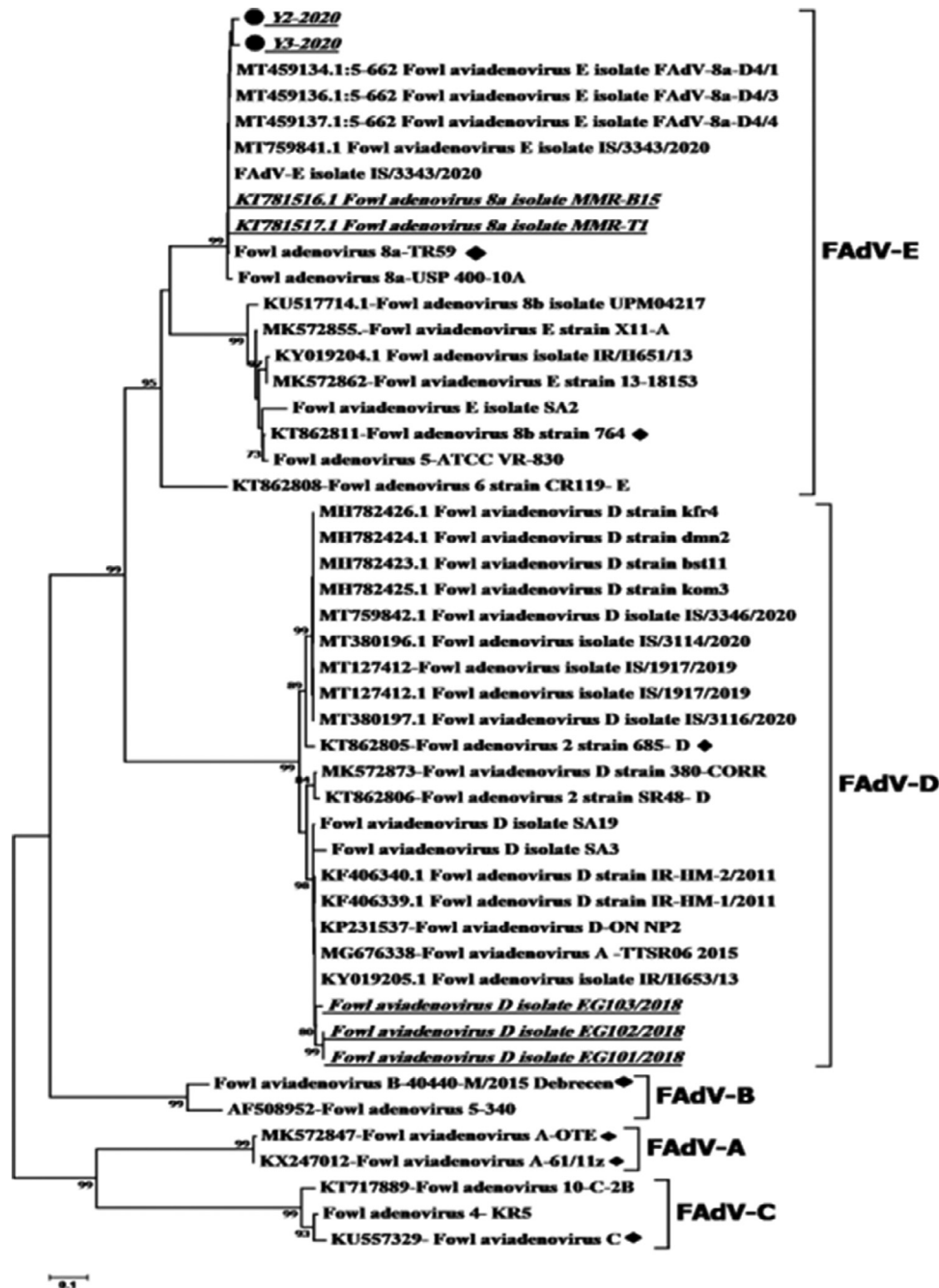


Figure 3. Phylogenetic tree of the nucleotide sequence of partial hexon gene of fowl adenovirus (FAdV), and the targeted strains (Y1 and Y2) were labeled with a black circle. The Egyptian strains were underlined in bold italic format. The targeted strains were genetically related to the Egyptian strains in 2018 and Israeli and Iranian strains in 2020–2021, which belonged to FAdV serotype 8a/E.

caused by marked hypercellularity in the glomerular spaces caused by mesangial cells and podocytes proliferation (Figure 7).

- Cardiac myofibers: The histological structure of cardiac myocytes in group C was normal with bundles of muscle fibers aggregated together. Within each myofiber, the myocardium had cylindrical, branching cells with a centrally located nucleus. However, moderate changes were observed in groups A and B. At 5 DPI, the cardiac myocytes appeared thin and dispersed with abundant edema. In a different sacrifice, group A had less mononuclear inflammatory cells infiltrations (5–21 DPI). Similar changes were observed in group B,

however, the lesions in this group appeared to be more severe than those in group A. At 5 DPI, there was significant interstitial edema which was followed by cardiac myocytes separation and a marked cardiomyopathy effect. The following sacrifices revealed multifocal areas of inflammatory cells aggregations, accompanied by fragmentation of the adjacent myofibers (Figure 8).

- Pancreas: Group C exhibited intact exocrine pancreatic acini made up of tubuloacinar glands with normal triangular epithelial cells. At 4 to 15 DPI, examination of groups A and B revealed multifocal areas of eosinophilic tissue debris replacement of pancreatic exocrine acini, infiltration of mononuclear

Table 1. Similarity % among the different serotypes of fowl adenovirus (FAdv). Y2 and Y3 the target of the current study were highly similar to serotype 8a – E with identity% = 97.8–98%.

Seq->	1	2	3	4	5	6	7	8	9	10	11	12	13	14	15	16	17	18	19	20	21
1 Y2-2020		98.9%	99.3%	99.5%	99.5%	78.0%	76.5%	56.2%	56.2%	78.9%	78.9%	56.3%	56.5%	55.7%	55.3%	64.2%	63.8%	65.1%	67.7%	68.2%	67.9%
2 Y3-2020	98.9%		99.1%	99.3%	99.3%	77.8%	76.5%	56.2%	56.2%	78.7%	78.9%	56.1%	56.3%	55.7%	55.3%	63.8%	64.2%	64.4%	67.3%	67.7%	67.5%
3 KT862810-FAdV-8a strain TR59	99.3%	99.1%		99.7%	99.7%	78.5%	76.9%	56.4%	56.4%	78.9%	79.3%	56.5%	56.7%	56.0%	55.5%	64.2%	64.0%	65.1%	67.9%	68.4%	68.2%
4 FAdV-8a isolate MMRT1	99.5%	99.3%	99.7%		100.0%	78.5%	76.9%	56.4%	56.4%	79.1%	79.3%	56.5%	56.7%	56.0%	55.5%	64.4%	63.8%	65.1%	67.9%	68.4%	68.2%
5 AD13-2020-8a/E	99.5%	99.3%	99.7%	100.0%		78.5%	76.9%	56.4%	56.4%	79.1%	79.3%	56.5%	56.7%	56.0%	55.5%	64.4%	63.8%	65.1%	67.9%	68.4%	68.2%
6 AD16-2020-8b/E	78.0%	77.8%	78.5%	78.5%	78.5%		98.0%	51.4%	51.4%	76.7%	84.4%	55.2%	55.2%	51.6%	50.1%	65.3%	61.4%	62.9%	65.1%	65.5%	65.3%
7 KT862811-FAdV-8b strain 764	76.5%	76.5%	76.9%	76.9%	76.9%	98.0%		51.4%	51.4%	77.4%	85.0%	55.0%	55.0%	51.6%	50.1%	65.5%	61.0%	63.5%	64.6%	65.1%	64.9%
8 KT717889-FAdV-10 strain C2B	56.2%	56.2%	56.4%	56.4%	56.4%	51.4%	51.4%		100.0%	54.7%	54.4%	63.0%	63.0%	93.8%	91.5%	51.6%	56.2%	55.7%	52.9%	51.4%	51.6%
9 AF339923-FAdV-9 strain ATCC VR834	56.2%	56.2%	56.4%	56.4%	56.4%	51.4%	51.4%	100.0%		54.7%	54.4%	63.0%	63.0%	93.8%	91.5%	51.6%	56.2%	55.7%	52.9%	51.4%	51.6%
10 KT862808-FAdV-6 strain CR119 E	78.9%	78.7%	78.9%	79.1%	79.1%	76.7%	77.4%	54.7%	54.7%		83.5%	58.7%	58.7%	54.4%	53.1%	67.5%	64.7%	65.3%	69.2%	67.9%	67.7%
11 KT862809-FAdV-7 strain YR36	78.9%	78.9%	79.3%	79.3%	79.3%	84.4%	85.0%	54.4%	54.4%	83.5%		58.0%	58.5%	54.9%	53.3%	65.1%	63.6%	64.0%	66.6%	65.7%	65.5%
12 Z67970-FAdV-1-CELO	56.3%	56.1%	56.5%	56.5%	56.5%	55.2%	55.0%	63.0%	63.0%	58.7%	58.0%		98.8%	62.8%	61.2%	56.9%	58.8%	54.8%	55.0%	53.4%	53.7%
13 AD17-2020-A	56.5%	56.3%	56.7%	56.7%	56.7%	55.2%	55.0%	63.0%	63.0%	58.7%	58.5%	98.8%		62.8%	61.2%	56.7%	58.6%	54.8%	55.0%	53.4%	53.7%
14 FAdV-4 strain KR5	55.7%	55.7%	56.0%	56.0%	56.0%	51.6%	51.6%	93.8%	93.8%	54.4%	54.9%	62.8%	62.8%		94.5%	51.8%	54.7%	54.9%	52.5%	51.6%	51.8%
15 FAdV-4/C-Egypt	55.3%	55.3%	55.5%	55.5%	55.5%	50.1%	50.1%	91.5%	91.5%	53.1%	53.3%	61.2%	61.2%	94.5%		50.5%	54.3%	55.1%	52.0%	50.5%	50.7%
16 KT862807-FAdV-6 strain SR49	64.2%	63.8%	64.2%	64.4%	64.4%	65.3%	65.5%	51.6%	51.6%	67.5%	65.1%	56.9%	56.7%	51.8%	50.5%		62.1%	66.6%	71.9%	68.8%	69.0%
17 AD19-2020-B	63.8%	64.2%	64.0%	63.8%	63.8%	61.4%	61.0%	56.2%	56.2%	64.7%	63.6%	58.8%	58.6%	54.7%	54.3%	62.1%		61.9%	61.4%	61.4%	61.6%
18 FAdV-5 strain TR22 B	65.1%	64.4%	65.1%	65.1%	65.1%	62.9%	63.5%	55.7%	55.7%	65.3%	64.0%	54.8%	54.8%	54.9%	55.1%	66.6%	61.9%		60.7%	59.6%	59.8%
19 KT862806-FAdV-2 strain SR48 D	67.7%	67.3%	67.9%	67.9%	67.9%	65.1%	64.6%	52.9%	52.9%	69.2%	66.6%	55.0%	55.0%	52.5%	52.0%	71.9%	61.4%	60.7%		92.4%	92.7%
20 FAdV-D-11-strain dmn2	68.2%	67.7%	68.4%	68.4%	68.4%	65.5%	65.1%	51.4%	51.4%	67.9%	65.7%	53.4%	53.4%	51.6%	50.5%	68.8%	61.4%	59.6%	92.4%		99.7%
21 AD1-2019-D	67.9%	67.5%	68.2%	68.2%	68.2%	65.3%	64.9%	51.6%	51.6%	67.7%	65.5%	53.7%	53.7%	51.8%	50.7%	69.0%	61.6%	59.8%	92.7%	99.7%	

inflammatory cells in the interstitial tissue, and the presence of deeply basophilic intranuclear inclusion bodies in the acinar epithelial cells (Figure 8).

- Bursa of Fabricius: In all sacrifices, group C (control group) showed a normal histological structure of the bursa of Fabricius. The bursa had a normal serosal covering, a smooth muscle layer, and an intact inner mucosa made up of pseudostratified columnar epithelial cells. The lymphoid follicles appeared normal with an outer cortex and inner medulla.

- The examination of groups A and B revealed various histopathological changes among different sacrifices. The observed lesions were more intense and occurred earlier in group B than in group A. At 4 DPI, some examined sections showed abundant exudation of mucin-like substances with tissue debris in the lumen of the bursa of chicks from group B.
- At 4 to 5 DPI lymphoid follicles depletion began in groups A and B. The follicles in group B, were severely depleted which was accompanied by cystic space formations with the accumulation of proteinaceous fluid, nuclear debris, and inflammatory cells infiltration within the destroyed lymphoid follicles. Destruction of lymphoid cells continued during the

Table 2. Results of fowl adenovirus shedding in cloacal swabs.

Days post-infection (DPI)	Groups	Virus shedding in cloacal swabs
3	A	Negative
	B	Negative
	C	Negative
5	A	Negative
	B	Negative
	C	Negative
7	A	Positive = 19.3
	B	Negative
	C	Negative
11	A	Positive = 26.9
	B	Positive = 21.2
	C	Negative
15	A	Positive = 27.5
	B	Positive = 25.8
	C	Negative
21	A	Positive = 26.1
	B	Negative
	C	Negative
24	A	Positive = 27.6
	B	Negative
	C	Negative

Syber green-based real-time quantitative polymerase chain reaction detected fowl adenovirus in the samples collected from the three groups of the experiment during 3, 5, 7, 11, 15, 21, and 24 DPI. The swabs possessed positivity in group A from the 7 DPI till 24 DPI, and group B was positive at 11 and 15 DPI, while the negative control group C was totally negative.

**Figure 4.** Liver of experimentally infected chicks showed paleness with hemorrhage.



Figure 5. Affected heart of experimentally infected birds with petechial hemorrhage.

following sacrifices. Numerous heterophils were found in the affected follicles of group A at 21 DPI and in group B at 15 DPI, and atrophied bursae were observed in group A which were characterized by a decreased number of lymphoid follicles associated with plica folding. At 24 DPI, group B demonstrated

severe depletion in numerous follicles as evidenced by the presence of a prominent zone of epithelial cells between the medulla and cortex (Figure 9).

- Lungs: The lung from group C had a normal histological structure with primary bronchi, secondary bronchi, and parabronchi. All examined chicks had intact respiratory lobules which were made up of tertiary bronchi, atria, infundibula, and air capillaries separated by thin interstitial tissue. At 5 DPI, perivascular edema with less inflammatory cell infiltration was observed in group A. At 9 to 11 DPI, secondary bronchi showed an accumulation of inflammatory cells, tissue debris, and desquamated epithelial cells in the bronchiolar lumen. At 18 DPI, an intense inflammatory response was observed in the interstitial tissue and secondary bronchi, which was accompanied by numerous multinucleated giant cell formations in the lumen of the secondary bronchi at 24 DPI. Group B had a strong immune response to adenovirus infection. At 4 DPI, proliferation of smooth muscle cells with epithelial hyperplasia and metaplasia was observed in the tertiary bronchi of affected chicks. Severe bronchopneumonia began at 9 DPI and was characterized by heavy mucous exudates, massive mononuclear inflammatory cells infiltration, and

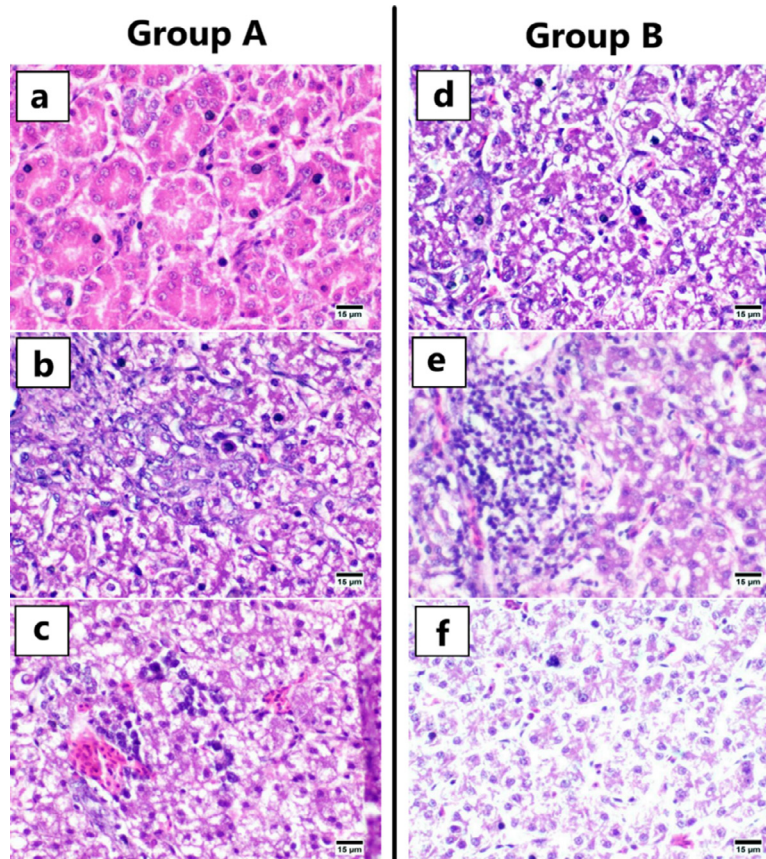


Figure 6. Photomicrograph of group A and B liver at different sacrifices (H & E). Variable number of intranuclear inclusion bodies in the affected hepatocytes, group A at 4 DPI (A). Vacuolation of hepatic plates with basophilic inclusion bodies filling the nuclei of infected hepatocytes, group A at 5 DPI (B). Few inflammatory cells infiltrated the hepatic parenchyma, group A at 7 DPI (C). Focal area of hepatocellular degeneration and necrosis with enlarging the nuclei of infected hepatocytes with deeply basophilic inclusion bodies of adenovirus, group B at 5 DPI (D). Replacing of the necrosed hepatic plates with the increased number of inflammatory cells infiltration, group B at 7 DPI (E). Severe necrosis and disorganization of hepatic plates with the accumulation of eosinophilic tissue debris, group B at 15 DPI (F). Abbreviation: DPI, days post-infection.

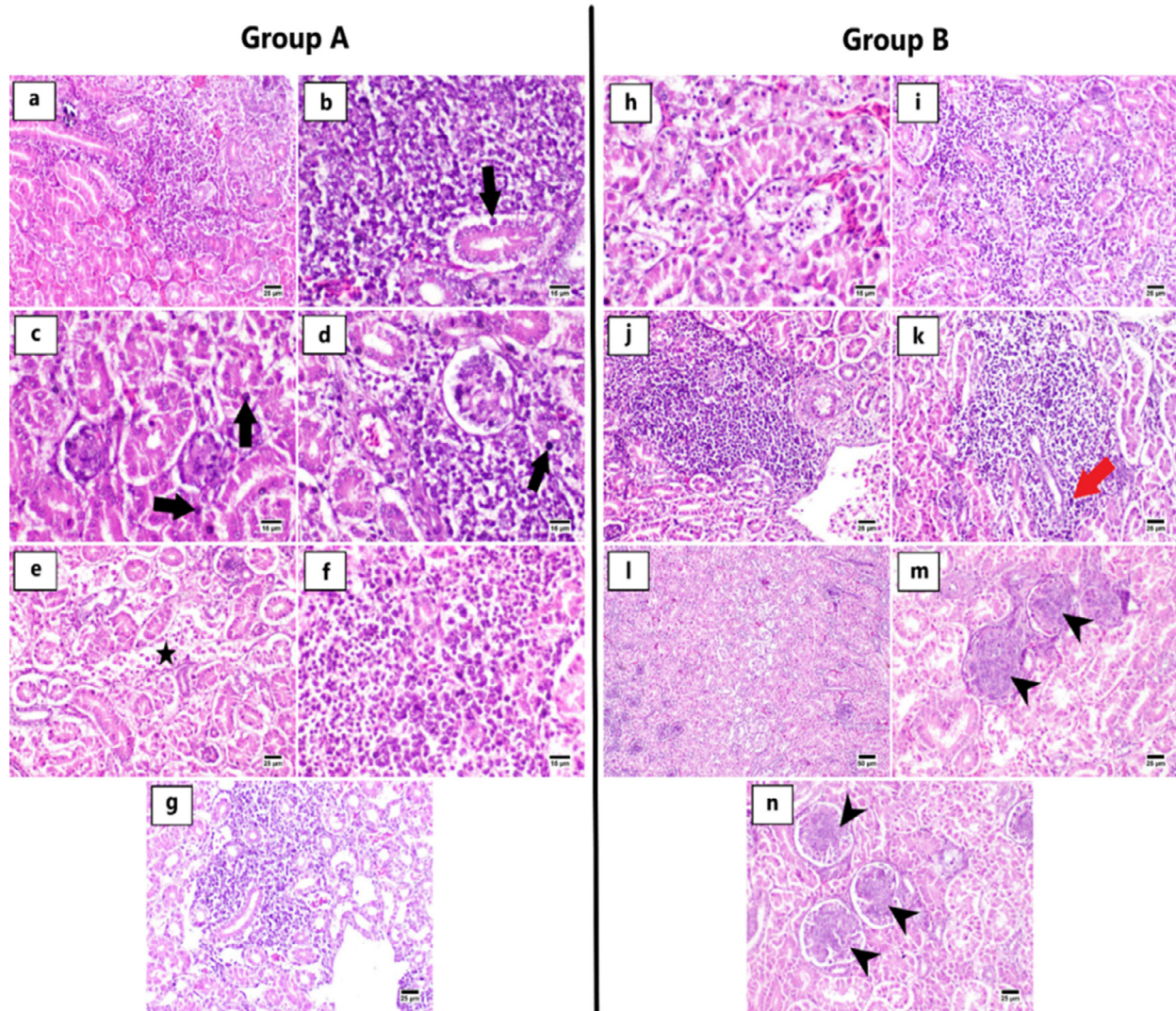


Figure 7. Photomicrograph of kidneys of group A and B at different sacrifices (H & E). Focal interstitial nephritis, group A at 4 DPI (A). Heavy peritubular mononuclear inflammatory cells accumulation admixed with basophilic intranuclear inclusion body in the epithelial lining renal tubule (black arrow), group A at 5 DPI (B). The variable number of intranuclear inclusion bodies (black arrows) with few necrosis in the renal tubules, group A at 5 DPI (C). Periglomerular aggregations of inflammatory cells with basophilic intranuclear inclusion body in the lining renal tubular epithelium (black arrow), group A at 5 DPI (D). Necrosis of epithelial lining renal tubules with sloughing of epithelial cells into the tubular lumen (star), group A at 7 DPI (E). Higher magnification of mononuclear inflammatory cells infiltrate the renal interstitial tissue associated with presence of inclusion bodies, group A at 9 DPI (F). Focal interstitial nephritis replacing necrotic tubules, group A at 24 DPI (G). Pyknosis and necrosis of epithelial lining renal tubules, group B at 5 DPI (H). Multifocal interstitial nephritis in the renal parenchyma replacing the affected renal tubules, group B at 5 DPI (I, J). Heavy mononuclear inflammatory cells accumulate in the renal interstitial tissue admixed with basophilic intranuclear inclusion bodies (red arrow), group B at 11 DPI (K). Widespread necrosis of renal tubules in the cortical region, group B at 15 DPI (L). Presence of mesangio-proliferative glomerulopathy (arrow heads) in the affected renal glomeruli in group B at 21 and 24 DPI, respectively (M, N). Abbreviation: DPI, days post-infection.

several scattered multinucleated giant cells with basophilic intranuclear inclusion bodies at 9 to 15 DPI (Figure 10).

- Statistical analysis (Figure 11) revealed significant differences in the proportion of birds with microscopic lesions in the liver, kidneys, and bursa between the uninfected group and inoculated groups.

Detection of Virus Shedding by Syber Green-Based Real-Time Quantitative PCR

The swabs in group A were positive at 7 to 24 DPI, those in group B were positive only at 11 and 15 DPI, and those in group C were completely negative.

DISCUSSION

In the current study, we examined birds suspected of having IBH and documented typical IBH signs and gross findings (Laanani et al., 2015). Of the 15 liver samples tested, two were positive when the hexon gene primer was used. The hexon gene is a major capsid protein that contains determinants from different groups and subgroups (Harrach et al., 2012; Schachner et al., 2016).

The hexon gene was sequenced and analyzed, and a phylogenetic tree based on the neighbor-joining method was constructed using a sequence assembly from reference FAdV isolates from various geographical locations. The analysis revealed that two isolates (MW574967, MW574968) belonged to serotype 8a, FAdVE species.

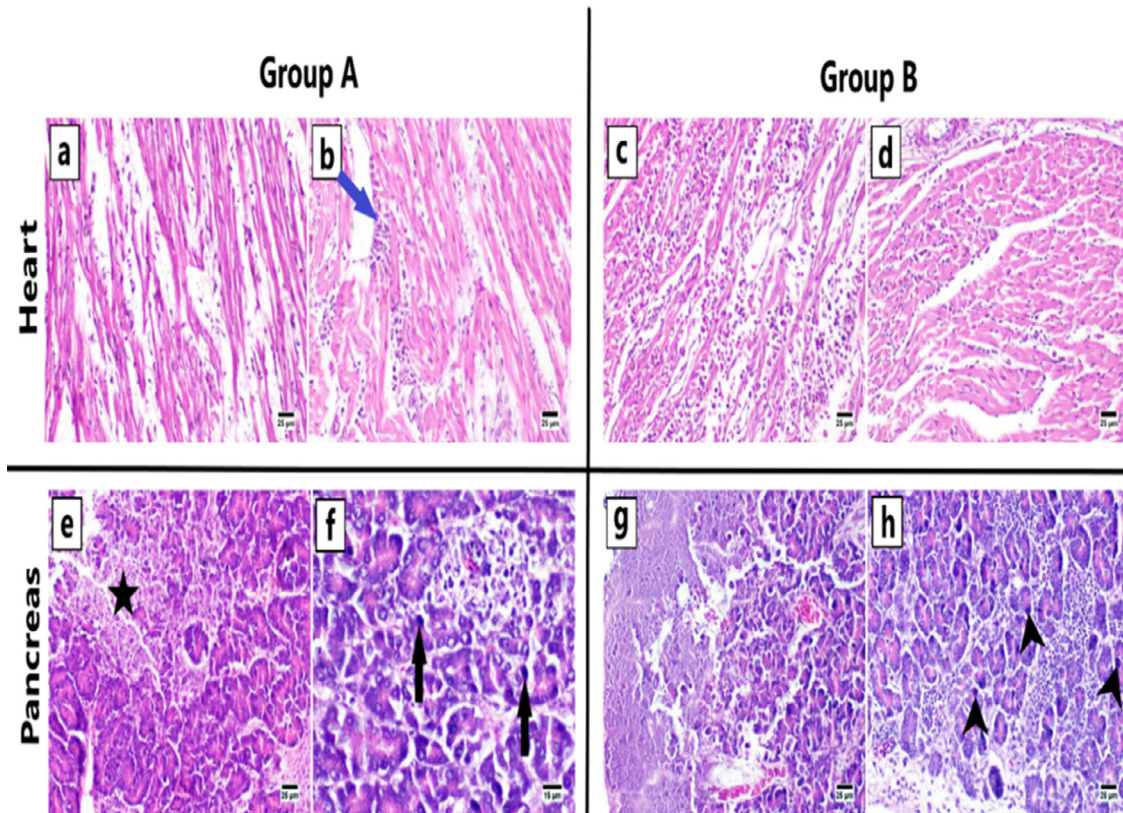


Figure 8. Photomicrograph of heart and pancreas of group A and B at different sacrifices (H & E). Dispersion of cardiac myocytes with edema and few inflammatory cells infiltration admixed with thinning of myocytes in group A at 5 DPI (A). Mild myocarditis with fewer inflammatory cells infiltration between myofibers (blue arrow) in group A at 21 DPI (B). Severe myocarditis admixed with marked cardiomyopathy in group B at 5 DPI (C). The variable number of mononuclear inflammatory cells infiltration associated with fragmentation of cardiac myocytes in group B at 15 DPI (D). Necrosis of pancreatic exocrine acini with the accumulation of eosinophilic tissue debris (star) in group A at 4 DPI (E). Presence of the variable number of deeply basophilic intranuclear inclusion bodies in the acinar epithelium (black arrows), group A at 9 DPI (F). Widespread necrotic pancreatic tissue, group B at 5 DPI (G). There are numerous basophilic intranuclear inclusion bodies in the lining epithelium of exocrine acini (black arrowheads), group B at 5 DPI (H). Abbreviation: DPI, days post-infection.

Mega 7 software was used to create a neighbor-joining phylogenetic tree based on 48 nucleotide sequences from different FAdV serotypes representing the five species A-E.

The phylogenetic tree revealed that our targeted strains Y1 and Y2 were genetically related to the serotype 8a/E. In addition, the two strains were also similar to the Egyptian strains isolated in 2018 (MMR-B15 and MMR-T1). They were also related to the Israeli and Iranian strains that were in circulation in 2020–2021. Radwan et al. (2019) isolated FAdV species E serotype 8a from the cloacal swabs of affected flocks but were unable to detect the virus in livers. This is the first study in which an Egyptian FAdV isolate underwent isolation, identification, and molecular characterization, with its pathogenicity characterized.

Concurrently, El basrey et al. (2020) discovered FAdV species D serotype 2. El-Tholoth and Abou El-Azm (2019) discovered FAdV species D in Kafr El Sheikh, Egypt in 2017. Another recent study reported the first case of FAdV-4 in Egypt (Sultan et al., 2021), and the recorded case was isolated from a Cobb broiler flock at 32 d of age in Alexandria with 15% mortality. Furthermore, Adel et al. (2021) discovered the emergence of new FAdV serotypes 1, 3, and 8b in Egypt for the first time.

We attempted to isolate the viruses from two positive samples by inoculating them in CELC and CPE was noted within 3 d. Several researchers have attempted to conduct isolation trials of FAdV in CELC and been successful in virus adaptation (Kataria et al., 1997; Barua and Rai, 2003). The FAdV was propagated in primary CELC in the current study, and the virus caused rounding, degeneration, and detachment of the infected cells from the monolayer, as observed by many other previous researchers (Balamurugan et al., 2002; Soumyalekshmi et al., 2014; Xie et al., 2020). The pathogenesis of the isolated strains was demonstrated in one-day-old commercial broiler chickens via the oral route in the present study. During the experimental period, neither mortality nor clinical signs were observed.

Even though the FAdV strains used in our study were isolated from commercial chickens and showed clinical signs, infection with these viruses showed no clinical signs. These findings confirmed that the outcome of FAdV infection is affected by various factors such as the bird's age, genetic background, experimental versus field condition, and route of inoculation. Matos et al. (2016a) were the first to report a substantial difference in the susceptibility of SPF broiler chickens to oral infection with FAdV strains from species D and E in comparison to SPF layers.

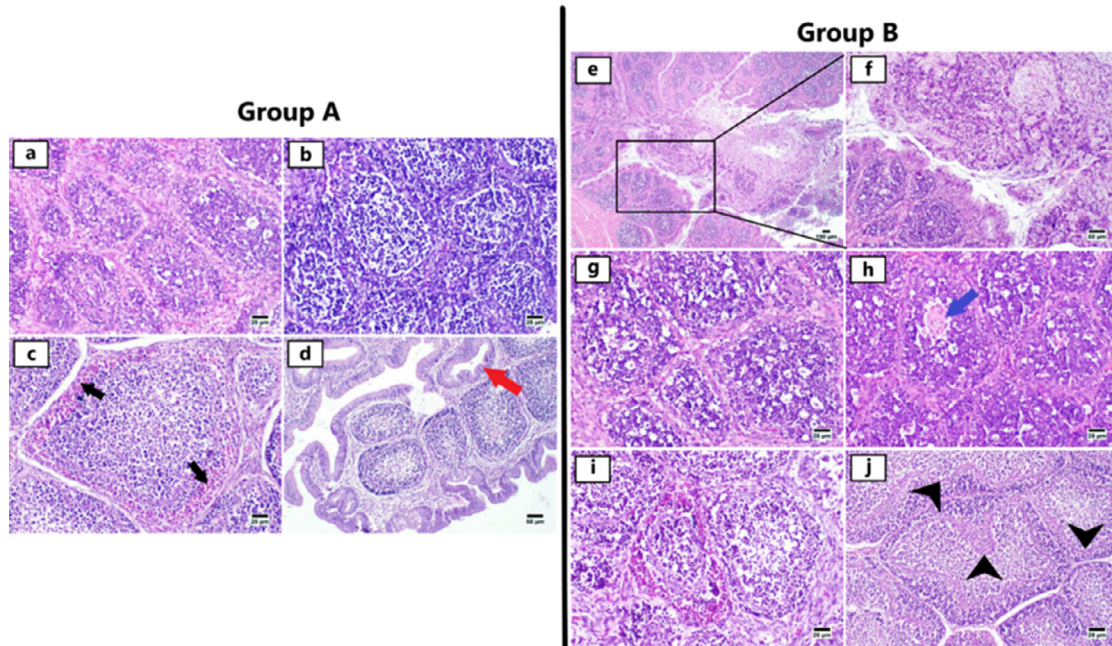


Figure 9. Photomicrograph of bursa of Fabricius of group A and B at different sacrifices (H & E). Mild to moderate depleted lymphoid follicles in group A at 4 DPI (A). Depleted follicles with variable number of inflammatory cells infiltration in the interfollicular tissue, group A at 5 DPI (B). Heterophilic infiltration in the cortex of lymphoid follicle (black arrows), group A at 21 DPI (C). Folding of the plica with presence of ductal structure resemble the epithelium lining the mucosa (red arrow), group A at 21 DPI (D). Excessive mucin like substance occupying the lumen of bursa of Fabricius, group B at 4 DPI (E). A higher magnification of the previous figure showing lumen filled with abundant exudates admixed with nuclear debris and desquamated epithelial cells, group B at 4 DPI (F). Numerous depleted follicles associated with expansion of the interfollicular tissue with edema and few inflammatory cells infiltration, group B at 4 DPI (G). Presence of proteinaceous fluid, debris and inflammatory cells in a damaged lymphoid follicle (blue arrow), group B at 5 DPI (H). A rim of heterophils infiltrated the cortex of lymphoid follicle, group B at 15 DPI (I). Presence a clear zone of epithelial cells between cortex and medulla of several affected follicles (black arrow heads), group B at 24 DPI (J). Abbreviation: DPI, days post-infection.

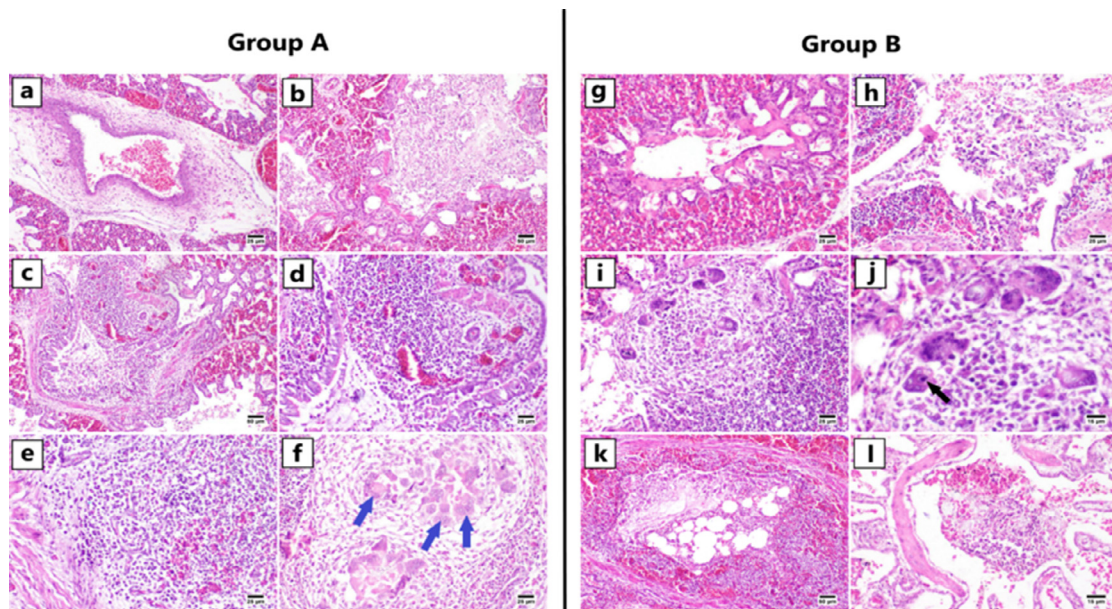


Figure 10. Photomicrograph of lungs of group A and B at different sacrifices (H & E). Excessive perivascular edema with fewer inflammatory cells infiltration, group A at 5 DPI (A). Accumulation of eosinophilic tissue debris in the bronchiolar lumen, group A at 9 DPI (B). Numerous inflammatory cells infiltration in the lumen of secondary bronchi, group A at 11 DPI (C). Higher magnification showed inflammatory cells infiltration in the submucosa admixed with severely congested blood vessels, group A at 11 DPI (D). Focal area of severe interstitial pneumonia, group A at 18 DPI (E). Existence of numerous multinucleated giant cells (blue arrows) in the bronchiolar lumen, group A at 24 DPI (F). Proliferative response in lung tissue showing smooth muscle hypertrophy associated with increased cellularity around the parabronchus, group B at 4 DPI (G). Accumulation of necrotic debris with inflammatory cells infiltration in the lumen of secondary bronchi, group B at 5 DPI (H). Numerous inflammatory cells with multinucleated giant cells occupying the lumen of parabronchus, group B at 15 DPI (I). Higher magnification showing deeply basophilic intranuclear inclusion bodies in the giant cells (black arrow), group B at 15 DPI (J). Occlusion of the lumen of secondary bronchus with intense inflammatory exudates, group B at 15 DPI (K). Hypertrophy of smooth muscle admixed with accumulation of inflammatory cells in the lumen of tertiary bronchus, group B at 24 DPI (L). Abbreviation: DPI, days post-infection.

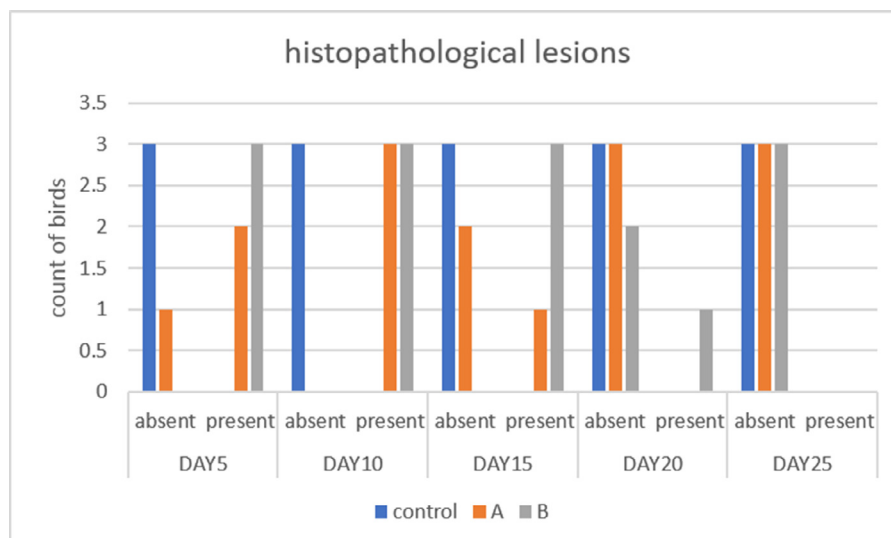


Figure 11. The proportion of birds in each experimental group. Histological lesions in each tissue examined was significantly different from uninfected group and inoculated group.

Okuda et al. (2004) observed no clinical signs after oral inoculation of serotype 8 in 5-day-old chicks and was unable to reisolate the virus from inoculated chicks' liver and pancreas. Even though they observed mortalities with severe clinical signs after intramuscular injection and the virus was isolated from the liver and the pancreas. Natural disease induction is difficult, whereas some studies have successfully reproduced IBH via unnatural inoculation routes such as intramuscular, intravenous, and intraabdominal routes (McFerreran, 1997). Although gross and histopathological examination of the birds revealed severe hepatitis with basophilic intranuclear inclusion bodies, Radwan et al. (2019) found no mortality in the infected group. It is well known that FAdV pathogenicity can range from mild infections to severe diseases (Zhao et al., 2016).

The outcome of experimental studies is highly dependent on the route of inoculation, viral dose, and age of birds. Age-related resistance is a distinct feature of avian adenoviral infections (Nakamura et al., 2000; Lim et al., 2011). In our study, we found a link between macroscopic lesions and histological findings. The current study also showed viral load in birds' droppings inoculated with serotype E. Despite the absence of clinical signs, birds inoculated with the two viruses excreted the virus via cloacal shedding throughout the experiment.

The experimental infection results showed that infected birds' droppings were a significant source of infection via the oral route of contaminated feed. Horizontal transmission of different FAdV serotypes was also observed in other clinical trials (Ono et al., 2007; Matos et al., 2016b). Furthermore, the amount and duration of virus shedding in the feces did not correlate with the pathogenicity of an individual strain, but rather with the viral dose administered (Matos et al., 2016b; Oliver-Ferrando et al., 2017).

Histopathological examination of livers revealed the most prominent lesion, basophilic intranuclear inclusion

bodies in hepatocytes, as reported by Dar et al. (2012) and Zhao et al. (2016). Other studies discovered nuclear eosinophilic inclusion bodies in hepatocytes, as well as hepatocytes degeneration and necrosis and inflammatory cells infiltration (Wang et al., 2020). Saifuddin and Wilks (1990) described hepatic necrosis with basophilic and eosinophilic inclusion bodies in hepatocytes nuclei. Shinde et al. (2020) detected the presence of intranuclear basophilic or eosinophilic inclusion bodies. Cardiac myocytes appeared thin and dispersed, with abundant edema, mononuclear inflammatory cells infiltration, and cardiomyopathy (Ahamad et al., 2017; Dutta et al., 2017).

The pancreas exhibited mononuclear inflammatory cells infiltration in the interstitial tissue, as well as the presence of deeply basophilic intranuclear inclusion bodies (El-atrache and Villegas, 2001; Matos et al., 2016a). Interstitial nephritis in the kidneys began at 4 DPI with the presence of basophilic intranuclear inclusion bodies, necrosis of the epithelial lining of renal tubules, and mesangial proliferative glomerulopathy at 21 to 24 DPI. Simultaneously, Matos et al. (2016a) demonstrated no histological changes in kidneys. Zhao et al. (2016) discovered protein casts in renal tubules and extensive congestion in the renal interstitial. However, Toro et al. (1999) observed swelling with generalized hyperemia.

CONCLUSIONS

In the present study, two strains of FAdV serotype E were isolated and their pathogenicity in broiler chickens was investigated. It was concluded that avian adenoviruses are economically significant owing to various disease conditions, such as IBH, which can occur in chickens as primary pathogens. Further research and a study on the possibility of developing a vaccine to limit the losses caused by the virus are warranted.

ACKNOWLEDGMENTS

The authors extend their appreciation to the Deanship of Scientific Research at Princess Nourah bint Abdulrahman University, Riyadh, Saudi Arabia, for supporting this research work.

Author contributions: M.L., M.R.M. M.M.R., and K. A. El-T conceived, designed the experiments. M.L., M. R.M. M.M.R. carried out the methodology section. M. S., A.A. and Y.F.H.E. organized, interpreted and analyzed the data using the statistical program software. M. T.E.-S., D.S.A., A.S.J. and K.A. El-T. wrote the original draft. N.M.A., M.T.E.-S and K.A. El-T wrote, reviewed and edited the final version of the manuscript. All authors have read and approved the final manuscript.

DISCLOSURES

The authors declare that the research was conducted in the absence of any commercial or financial relationships that could be construed as a potential conflict of interest.

REFERENCES

- Adair, B. M., and J. A. Smyth. 2008. Group I adenovirus infections. Pages 252–266 in *Diseases of Poultry*. Y. M. Saif, A. M. Fadly, J. R. Glisson, L. R. McDougald, L. K. Nolan and D. E. Swayne, eds. Iowa State University Press, Ames, IA, USA.
- Adel, A., A. A. Mohamed, M. Samir, N. M. Hagag, A. Erfan, M. Said, A. Arafa, W. M. Hassan, M. E. El Zowalaty, and M. A. Shahien. 2021. Epidemiological and molecular analysis of circulating fowl adenoviruses and emerging of serotypes 1, 3, and 8b in Egypt. *Heliyon* 7:e08366.
- Ahamad, D. B., J. Selvaraj, M. Sasikala, and N. B. Prasath. 2017. Pathological study of an outbreak of hydropericardium syndrome in Giriraja chicken. *Indian J. Vet. Pathol.* 41:53–56.
- Balamurugan, V., J. M. Kataria, R. S. Kataria, K. C. Verma, and T. Nanthakumar. 2002. Characterization of fowl adenovirus serotype-4 associated with hydropericardium syndrome in chicken. *Comp. Immunol. Microbiol. Infect. Dis.* 25:139–147.
- Barua, S., and A. Rai. 2003. Cultivation of fowl adenovirus-4 in chicken embryo liver cell culture and purification of the virus by ultracentrifugation. *Indian J. Comp. Microbiol. Immunol. Infect. Dis.* 24:195–196.
- Benko, M., B. Harrach, G. W. Both, W. C. Russel, B. M. Adair, E. Adam, J. C. de Jong, M. Hess, M. Johnson, A. Kajan, A. H. Kidd, H. D. Lehmkuhl, Q.-G. Li, V. Mautner, P. Pring-Akerblom, and G. Wadell. 2005. Family adenoviridae. Pages 213–228 in *Virus Taxonomy*. Eighth Report of the International Committee on the Taxonomy of Viruses. C. M. Fauquet, J. Maniloff and L. A. Ball, eds. Elsevier Academic Press, New York, NY.
- Choi, K. S., S. J. Kye, J. Y. Kim, W. J. Jeon, E. K. Lee, K. Y. Park, and H. W. Sung. 2012. Epidemiological investigation of outbreaks of fowl adenovirus infection in commercial chickens in Korea. *Poult. Sci.* 91:2502–2506.
- Dar, A., S. Gomis, I. Shirley, G. Mutwiri, R. Brownlie, A. Potter, V. Gerdt, and S. K. Tikoo. 2012. Pathotypic and molecular characterization of a fowl adenovirus associated with inclusion body hepatitis in Saskatchewan chickens. *Avian Dis.* 56:73–81.
- Dutta, B., P. Deka, S. Gogoi, M. Sarmah, M. Bora, and D. Pathak. 2017. Pathology of inclusion body hepatitis hydropericardium syndrome (IBH-HPS) in broiler chicken. *Int. J. Chem. Stud.* 5:458–461.
- El basrey, Y. F., R. I. Hamed, M. Mohamed, and M. A. Lebdah. 2020. Detection of inclusion body hepatitis virus in broilers at Sharkia province. *Egypt. J. Anim. Health Prod.* 9:84–89.
- El-Attrache, J., and P. Villegas. 2001. Genomic identification and characterization of avian adenoviruses associated with inclusion body hepatitis. *Avian Dis.* 45:780–787.
- Elbestawy, A. R., M. Ibrahim, H. Hammam, A. E. Noreldin, A. El Bahrawy, and H. F. Ellakany. 2020. Molecular characterization of fowl adenovirus d species in broiler chickens with inclusion body hepatitis in Egypt. *AJVS* 64:110–117.
- El-Tholoth, M., and K. I. Abou El-Azm. 2019. Molecular detection and characterization of fowl adenovirus associated with inclusion body hepatitis from broiler chickens in Egypt. *Trop. Anim. Health. Prod.* 51:1065–1071.
- Eregae, M. E., C. E. Dewey Dewey, S. A. McEwen, R. Ouckama, D. Ojkić, and M. T. Guerin. 2014. Flock prevalence of exposure to avian adeno-associated virus, chicken anemia virus, fowl adenovirus, and infectious bursal disease virus among Ontario broiler chicken flocks. *Avian Dis.* 58:71–77.
- Fitzgerald, S. D., S. Rautenschlein, H. M. Mahsoub, F. W. Pierson, W. M. Reed, and S. W. Jack. 2020. Adenovirus infections. Pages 321–363 in *Diseases of Poultry*. D. E. Swayne, M. Boulianne, C. M. Logue, L. R. McDougald, V. Nair and D. L. Suarez, eds. John Wiley & Sons, Inc, Hoboken, NJ.
- Harrach, B., and G. Kajan. 2011. Aviadenovirus. Pages 13–28 in *Aviadenoviridae*. G. Darai, S. Konle and J. Simniok, eds. Springer, Berlin, Germany.
- Harrach, B., M. Benkö, G. W. Both, M. Brown, A. J. Davison, M. Echavarria, M. Hess, M. S. Jones, A. Kajan, H. D. Lehmkuhl, V. Mautner, S. K. Mittal, and G. Wadell. 2012. Family adenoviridae. Pages 125–141 in *Virus Taxonomy: Ninth Report of the International Committee on Taxonomy of Viruses*. A. M. Q. King, M. J. Adams, E. B. Carstens and E. J. Lefkowitz, eds. Elsevier Academic Press, New York, NY.
- Hess, M. 2013. Aviadenovirus infections. Pages 290–300 in *Diseases of Poultry*. D. E. Swayne, J. R. Glisson, L. R. McDougald, L. K. Nolan, D. L. Suarez and V. Nair, eds. 13th ed. Wiley-Blackwell, Ames, IA.
- Kataria, J. M., K. C. Verma, S. J. Jadhao, J. N. Deepak, and R. L. Shah. 1997. Efficacy of an inactivated oil emulsified vaccine against inclusion body hepatitis-hydropericardium syndrome in chicken prepared from cell culture propagated fowl adenovirus. *Indian J. Comp. Microbiol. Immunol. Infect. Dis.* 18:38–42.
- Laanani, I., N. Alloui, O. Bennoune, W. Laabaci, A. Ayachi, and M. S. Benterki. 2015. Clinical and histopathological investigations on inclusion body hepatitis in chickens in the AinTouta Area (Algeria). *Global J. Ani. Sci. Res.* 3:72–76.
- Lim, T. H., H. J. Lee, D. H. Lee, Y. N. Lee, J. K. Park, H. N. Youn, M. S. Kim, H. S. Youn, J. B. Lee, S. Y. Park, I. S. Choi, and C. S. Song. 2011. Identification and virulence characterization of fowl adenoviruses in Korea. *Avian Dis.* 55:554–560.
- Matos, M., B. Grafl, D. Liebhart, and M. Hess. 2016a. The outcome of experimentally induced inclusion body hepatitis (IBH) by fowl aviadenoviruses (FAdVs) is crucially influenced by the genetic background of the host. *Vet Res.* 47:69.
- Matos, M., B. Grafl, D. Liebhart, I. Schwendenwein, and M. Hess. 2016b. Selected clinical chemistry analytes correlate with the pathogenesis of inclusion body hepatitis experimentally induced by fowl aviadenoviruses. *Avian Pathol.* 45:520–529.
- McFerran, J. B. 1997. Group I adenovirus infections. Pages 607–620 in *Diseases of poultry*. B. W. Calnek, H. J. Barnes, C. W. Beard, L. R. McDougald and Y. M. Saif, eds. 10th Ed. Iowa State University Press, Ames, IA.
- Meng, F., G. Dong, Y. Zhang, S. Tian, Z. Cui, S. Chang, and P. Zhao. 2018. Co-infection of fowl adenovirus with different immunosuppressive viruses in a chicken flock. *Poult. Sci.* 97:1699–1705.
- Morshed, R., H. Hosseini, A. G. Langeroudi, M. H. B. Fard, and S. Charkhkar. 2017. Fowl adenoviruses D and E cause inclusion body hepatitis outbreaks in broiler and broiler breeder pullet flocks. *Avian Dis* 61:205–210.
- Nakamura, K., M. Mase, S. Yamaguchi, and N. Yuasa. 2000. Induction of hydropericardium in one-day-old specific pathogen-free chicks by adenoviruses from inclusion body hepatitis. *Avian Dis.* 44:192–196.
- Niczyporuk, J. S. 2016. Phylogenetic and geographic analysis of fowl adenovirus field strains isolated from poultry in Poland. *Arch. Virol.* 16:33–42.

- Niu, Y., Q. Sun, G. Zhang, W. Sun, X. Liu, Y. Xiao, Y. Shang, and S. Liu. 2018. Epidemiological investigation of outbreaks of fowl adenovirus infections in commercial chickens in China. *Transbound. Emerg. Dis.* 65:e121–e126.
- Okuda, Y., M. Ono, I. Shibata, and S. Sato. 2004. Pathogenicity of serotype 8 fowl adenovirus isolated from gizzard erosions of slaughtered broiler chickens. *J. Vet. Med. Sci.* 66:1561–1566.
- Oliver-Ferrando, S., R. Dolz, C. Calderón, R. Valle, R. Rivas, M. Perez, M. Biarnes, A. Blanco, K. Bertran, A. Ramis, N. Busquets, and N. Majo. 2017. Epidemiological and pathological investigation of fowl aviadenovirus serotypes 8b and 11 isolated from chickens with inclusion body hepatitis in Spain (2011–2013). *Avian Pathol.* 46:157–165.
- Ono, M., Y. Okuda, I. Shibata, S. Sato, and K. Okada. 2007. Reproduction of adenoviral gizzard erosion by the horizontal transmission of fowl adenovirus serotype 1. *J. Vet. Med. Sci.* 69:1005–1008.
- Radwan, M. M., A. H. El-Deeb, M. R. Mousa, A. A. El-Sanousi, and M. A. Shalaby. 2019. First report of fowl adenovirus 8a from commercial broiler chickens in Egypt: molecular characterization and pathogenicity. *Poult. Sci.* 98:97–104.
- Reed, L. J., and H. Muench. 1938. A simple method of estimating fifty percent endpoints. *Am. J. Trop. M. Hyg.* 27:493–497.
- Saifuddin, M. D., and C. R. Wilks. 1990. Reproduction of inclusion body hepatitis in conventionally raised chickens inoculated with a New Zealand isolate of avian adenovirus. *N. Z. Vet. J.* 38:62–65.
- Schachner, A., A. Marek, B. Grafl, and M. Hess. 2016. Detailed molecular analyses of the hexon loop-1 and fibers of fowl aviadenoviruses reveal new insights into the antigenic relationship and confirm that specific genotypes are involved in field outbreaks of inclusion body hepatitis. *Vet. Microbiol.* 186:13–20.
- Schachner, A., A. Marek, B. Jaskulska, I. Bilic, and M. Hess. 2014. Recombinant FAdV-4 fiber-2 protein protects chickens against hepatitis-hydropericardium syndrome (HHS). *Vaccine* 32:1086–1092.
- Schachner, A., M. Matos, B. Grafl, and M. Hess. 2018. Fowl adenovirus-induced diseases and strategies for their control – a review on the current global situation. *Avian Pathol.* 47:111–126.
- Shinde, D. B., A. L. Thormoth, S. S. Koratkar, N. Sharma, A. Rajguru, V. Rale, P. Wagh, T. Y. Prajitno, and S. S. Tongaonkar. 2020. Molecular and pathotypic characterization of fowl adenovirus associated with inclusion body hepatitis in Indian chickens. *Res. Square* 1–12.
- Soumyalekshmi, S., M. K. Ajithand, and M. Chandraprakash. 2014. Isolation of fowl adenovirus in chicken embryo liver cell culture and its detection by hexon gene based PCR. *Indian J. Sci. Technol.* 2:33–36.
- Su, Q., Y. Li, F. Meng, Z. Cui, S. Chang, and P. Zhao. 2018. Newcastle disease virus- attenuated vaccine co-contaminated with fowl adenovirus and chicken infectious anemia virus results in inclusion body hepatitis-hydropericardium syndrome in poultry. *Vet. Microbiol.* 218:52–59.
- Sultan, H., A.-E. S. Arafa, A. Adel, K. Selim, M. El-Hoseni, and S. Talaat. 2021. Genetic characterization of novel fowl aviadenovirus-4 (FADV-4) from the outbreak of hepatitis hydropericardium syndrome in commercial broiler chickens in Egypt novel FAdV-4 in Egypt. *Avian Dis.* 65:385–390.
- Toro, H., C. Prusas, R. Raue, L. Cerda, C. Geisse, C. Gonzalez, and M. Hess. 1999. Characterization of fowl adenoviruses from outbreaks of inclusion body hepatitis/hydropericardium syndrome in Chile. *Avian Dis.* 43:262–270.
- Wang, J., I. Zaheer, M. K. Saleemi, X. Qi, Y. Gao, H. Cui, K. Li, L. Gao, A. Fayyaz, A. Hussain, C. Liu, Y. Zhang, X. Wang, and Q. Pan. 2020. The first complete genome sequence and pathogenicity characterization of fowl adenovirus 11 from chickens with inclusion body hepatitis in Pakistan. *Vet. Microbiol.* 244:108670.
- Xie, W., G. Liang, A. Huang, F. Zhang, and W. Guo. 2020. Comparative study on the mRNA expression of *Pinus massoniana* infected by *Bursaphelenchus xylophilus*. *J. For. Res.* 31:75–86.
- Zhang, H., W. Jin, K. Ding, X. Cheng, Y. Sun, J. Wang, and C. Zhang. 2017. Genetic characterization of fowl adenovirus strains isolated from poultry in China. *Avian Dis.* 61:341–346.
- Zhao, J., Q. Zhong, Y. Zhao, Y. Hu, and G. Zhang. 2016. Pathogenicity and complete genome characterization of fowl adenoviruses isolated from chickens associated with inclusion body hepatitis and hydropericardium syndrome in China. *PLoS One* 11:e0161744.